Bulletin of the Seismological Society of America, Vol. 78, No. 2, pp. 692–707, April 1988

HIGH-FREQUENCY SPECTRA OBSERVED AT ANZA, CALIFORNIA: IMPLICATIONS FOR Q STRUCTURE

By S. E. Hough and J. G. Anderson

Abstract

Data from the Anza array in southern California have been analyzed to yield a model for the depth dependence of attenuation. The result is obtained from a formal inversion of the distance dependence of the spectral decay parameter, κ, observed from sources at a wide range of distances from single stations.

The inversion procedure assumes constant Q_i in plane layers and finds models which are as nearly constant with depth as possible. We find that the data cannot be explained by a model in which Q_i is constant with depth and that the data generally require three-layer models. The resulting models typically give Q_i for P waves between 300 and 1000 in the top 5 km, rising to 1000 to 3000 at greater depths, and decreasing to 700 to 1000 around 12 km depth. Q_i for S waves is slightly higher in most cases. Because this depth dependence of Q_i is generally correlated with the depths of earthquake epicenters, we suggest that Q_i may be due to a pressure and temperature-controlled intrinsic attenuation mechanism.

Introduction

In a companion paper (Hough *et al.*, 1988), the specific attenuation parameter, Q, has been obtained from a set of 68 earthquakes recorded at the Anza, California, array. In addition, Hough *et al.* (1988) obtained for each seismogram a two-parameter characterization of the high-frequency asymptote of the acceleration spectrum

$$A(f) \sim A_0 e^{-\pi\kappa f}. \tag{1}$$

The zero-frequency asymptote (A_0) and the decay parameter (κ) are found from both the P- and S-wave spectra. Equation (1) was found to provide a good fit to the spectra for frequencies from 10 to as much as 100 Hz.

This paper assumes κ is caused by a frequency-independent contribution, Q_i, to Q. However, we go beyond the simple two-layer Q_i model described by Hough *et al.* (1988). We assume that Q_i is a general function of depth, z, and use the distance dependence of κ to invert for this depth dependence. In order to test the necessity of having structure in the $Q_i(z)$ models, we penalize deviations between the value of $Q_i^{-1}(z)$ in each layer and the mean value of Q_i^{-1}. We force the models to be as smooth as possible without allowing an unacceptable level of misfit between the model predictions and the observations. Finally, we show that the total attenuation (Hough *et al.*, 1988) can be approximated as a sum of the contribution from Q_i and $Q_d \sim a_d f$, derived from the distance dependence of A_0.

The frequency-dependent component of attenuation was derived from Hough *et al.* (1988). Assuming a $1/r$ contribution from geometrical spreading, a least-squares regression through data from stations KNW and PFO yielded

$$Q_{Sd}^{-1} = \frac{(0.019 \pm 0.003)}{f} \tag{2a}$$

$$Q_{Pd}^{-1} = \frac{(0.023 \pm 0.006)}{f} \tag{2b}$$

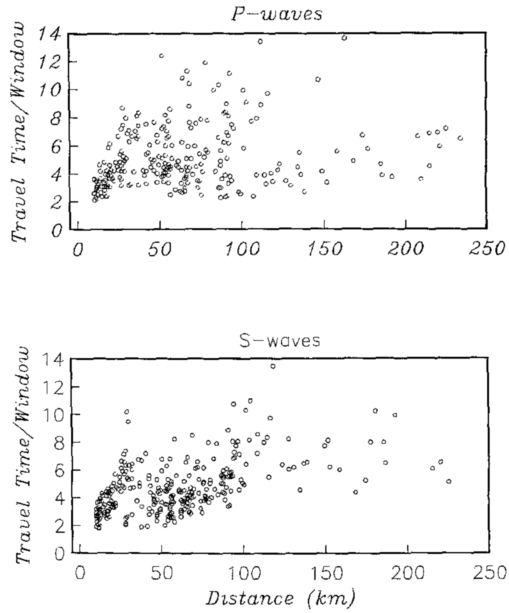

FIG. 1. The ratio of travel time to the first arrival versus time window length used in computing the spectra is shown for P and S waves as a function of epicentral distance.

where Q_{Sd} and Q_{Pd} are the frequency-dependent components of Q for S and P waves. These estimates apply to the depths where lateral propagation is taking place, i.e., greater than 10 km. We do not have any resolution of Q_d in the shallow part of the crust because this component of attenuation will lower the spectra uniformly without changing their shapes.

Method for Estimation of Q Structure

In order to relate the decay parameters to Q structure, we will assume that

$$\kappa(r) = \int_{path} \frac{dr}{Q_i(z)\beta(z)}. \tag{3}$$

We note that equation (3) is similar to the expression for t^*, but uses $Q_i(z)$ instead of the total $Q(z)$. As emphasized in Hough *et al.* (1988), the frequency-dependent contribution to Q does not affect $\kappa(r)$.

$\kappa(r)$ can be inverted for $Q_i(z)$ if the velocity model is known. The problem is linear in Q_i^{-1}. A velocity model with station corrections has been computed for the area using travel-time data (Vernon, personal communication). This model gives velocities to 18 km depth. Velocities at greater depth are taken from regional velocity studies (Doser and Kanamori, 1986). Thus, one can trace rays through the plane-layer velocity model, match each $\kappa(r)$ up with a ray, and invert for Q_i in plane layers, requiring $Q_i \geqq 0$. The sources are assumed to be at 12 km depth.

Our inversion procedure assumes that the first ray arrival is representive of all arrivals in our time window used for determining κ. This assumption is difficult to verify, although one measure of its validity is the ratio of the travel time of the first arrival versus the window length used. For example, using a single-scattering model, this ratio can be interpreted in terms of a maximum angular deviation from the first arrival ray path. This ratio can also be interpreted in terms of the range of group velocities included if all arrivals are assumed to travel the same distance.

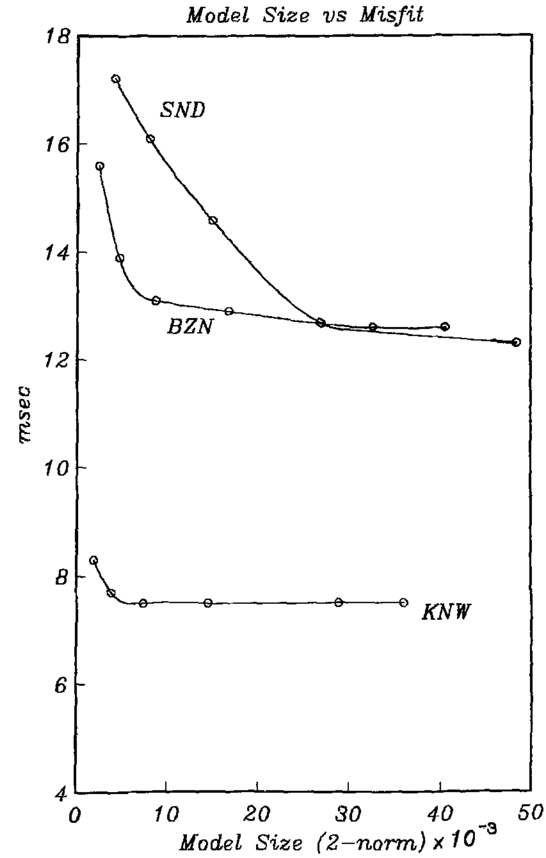

FIG. 2. Curves showing trade-off between model size and misfit, where model size is the 2-norm given by equation (4). Smoother models do not predict the observed values of κ as well as models with larger model size.

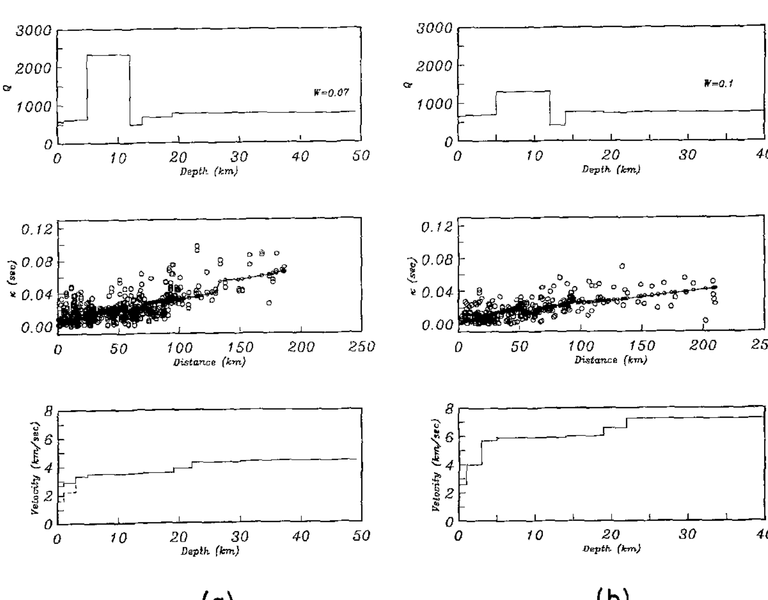

FIG. 3. Best-fitting Q_i model from combined S- and P-wave data. The data are shown along with the predicted values of κ given the Q_i model and velocity profile.

Figure 1 shows the ratio of travel time to window length for all S and P waves used in this study. We note that this ratio is at least two for almost all events studied.

Following the procedures presented by Backus and Gilbert (1968, 1970), one can invert for a Q_i model which optimizes certain qualities deemed to be desirable and test the resolution. One can find the models which yield minimal or maximal values of $\| Q_i \|_2$, the 2-norm of Q_i. As is frequently the case in inverse problems, a straightforward inversion leads to models which are unreasonably oscillatory. There are a number of ways that are used to impose one's prejudices in order to obtain physically reasonable models. The simplest, perhaps, is to penalize the derivative of the model. An alternative approach is to penalize the difference between each element in the model and the mean of the model. The latter procedure produces models which are as nearly constant with depth as possible. Utilizing the formalism presented by Stark *et al.* (1986), the problem for a surface source is expressed as follows

$$\min_{q \geqq 0} \left\| \begin{pmatrix} w_t L \\ M \end{pmatrix} \begin{pmatrix} \vec{q} \\ q_{ave} \end{pmatrix} - \begin{pmatrix} w_t \vec{\kappa}/2 \\ 0 \end{pmatrix} \right\|_2 \tag{4}$$

$$M = \begin{pmatrix} 1 & 0 & \cdot & \cdot & 0 & -1 \\ 0 & 1 & 0 & \cdot & 0 & -1 \\ \cdot & \cdot & \cdot & \cdot & \cdot & \cdot \\ 0 & \cdot & \cdot & \cdot & 1 & -1 \end{pmatrix} \tag{5}$$

$$L_{ij} = \frac{1}{\cos(\theta_{ij})\beta_i} \tag{6}$$

where θ_{ij} is the angle of the jth ray propagating through the ith layer, $\vec{\kappa}$ is a vector of length j of observed values of κ, $\vec{q}$ is a vector whose ith element is Q^{-1} in the ith

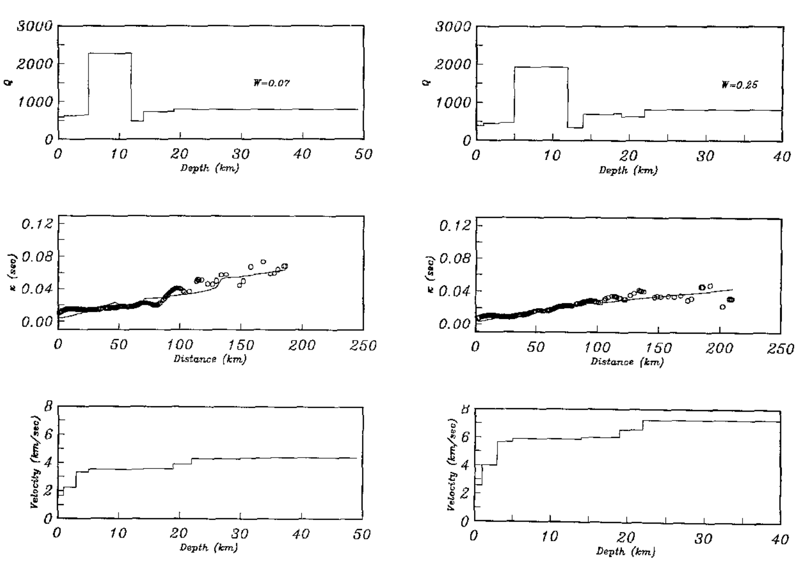

(a) (b)

FIG. 4. Q_i models from combined, smoothed data sets. $\kappa(r)$ values are smoothed over ±10 km.

layer, and q_{ave} is the unknown mean of the optimal model. The layer thickness is chosen to be 1 km. The dimensions of M are NLAY by (NLAY + 1), where NLAY is the number of layers in the Q_i model. L_{ij} is set to zero for j = NLAY + 1. In order to consider sources at depth, we take $L_{ij}* = \frac{1}{2} L_{ij}$ for segments of the ray path above the assumed source depth. w_t is a weight which can be used to produce smoother models if one is willing to tolerate larger misfit.

The choices of w_t are facilitated by examining the trade-off curves, shown in Figure 2 for S waves. In Figure 2, each circle represents the misfit and model size for a weight ranging from 0.05 at left to 1.0 at right. For all three stations, the sharp bend in the trade-off curves occurs for weights near 0.1. Model size refers to the size of the 2-norm given by equation (4), and misfit is the root mean square misfit between the model predictions and the data. Due to the long tails on these curves, one can obtain significantly smoother models, with little increase in misfit, by choosing w_t to be around 0.1 for S waves. The fact that these curves bend sharply up for $w_t < 0.1$ is noteworthy. As w_t decreases, the solution approaches a constant Q_i model [equation (4)], and the model size increases. The trade-off curves suggest that there is structure $Q_i(z)$ which is not well modeled if w_t is forced to be too low.

Application to Anza Data

We can invert combined data from all stations, making the appropriate travel-time correction for data at each station, as well as data from individual stations. The travel-time corrections are applied over the top 3 km of the velocity models. Figure 3 (a and b) shows inversion results for combined P- and S-wave data sets, and Figure 4 (a and b) shows results using combined data which has been smoothed over ±10 km. Since $\kappa(r)$ at each station is modeled to first order by a common trend plus a station correction, $\kappa(0)$, the scatter in the combined data sets is not representative of the uncertainty in the data. We consider the $Q_i(z)$ models presented in Figure 4 to be the preferred average results at Anza.

Figure 5 (a and b) shows $\kappa(r)$ observations, and Figure 6 (a and b) shows the inversion for $Q_i(Z)$ obtained from this unsmoothed data at each individual station. The average Q models from Figure 4 are superimposed on Figure 6. The $\kappa(r)$ curves corresponding to each Q model is shown in Figure 5.

The inversion shows two interesting results: (1) a tendency toward three-layer models, with Q_i for P waves ranging from 300 to 1000 in the upper 5 to 7 km, rising to 1000 to 3000 at greater depths, and dropping down to ≈1000 around 12 to 15 km. (2) Q_i for S waves is generally higher than for P waves. We note that the effect of attenuation is by an integral of t/Q, so that if Q_S/Q_P is equal to ν_P/ν_S, then the attenuation has the same effect on P and S waves. Our result for Q_S/Q_P (around 1.4) is slightly lower than the observed ν_P/ν_S ratio of ≈1.7. Thus, we do not contradict observations that observed waveforms show a greater level of high frequencies in the P wave than in the S wave.

The structure in the Q_i models can be explained in a qualitative way from the characteristic shape of $\kappa(r)$. The observed κ values at Anza are typically described by a small but nonzero intercept, $\kappa(0)$, a very low increase of κ to distances around 50 km, and a faster increase at greater distances. The nonzero intercept generally implies the low Q_i layer for $0 \leqq z \leqq 5$ km, the slow increase of κ at close distances implies a high Q_i at depths below 5 km, and the faster increase of κ requires a slightly lower Q_i layer at greater depths.

Looking at the observed data points in Figures 3 and 5, it is clear that some of the data sets are consistent with a $d\kappa/dr$ which is essentially zero between 10 and

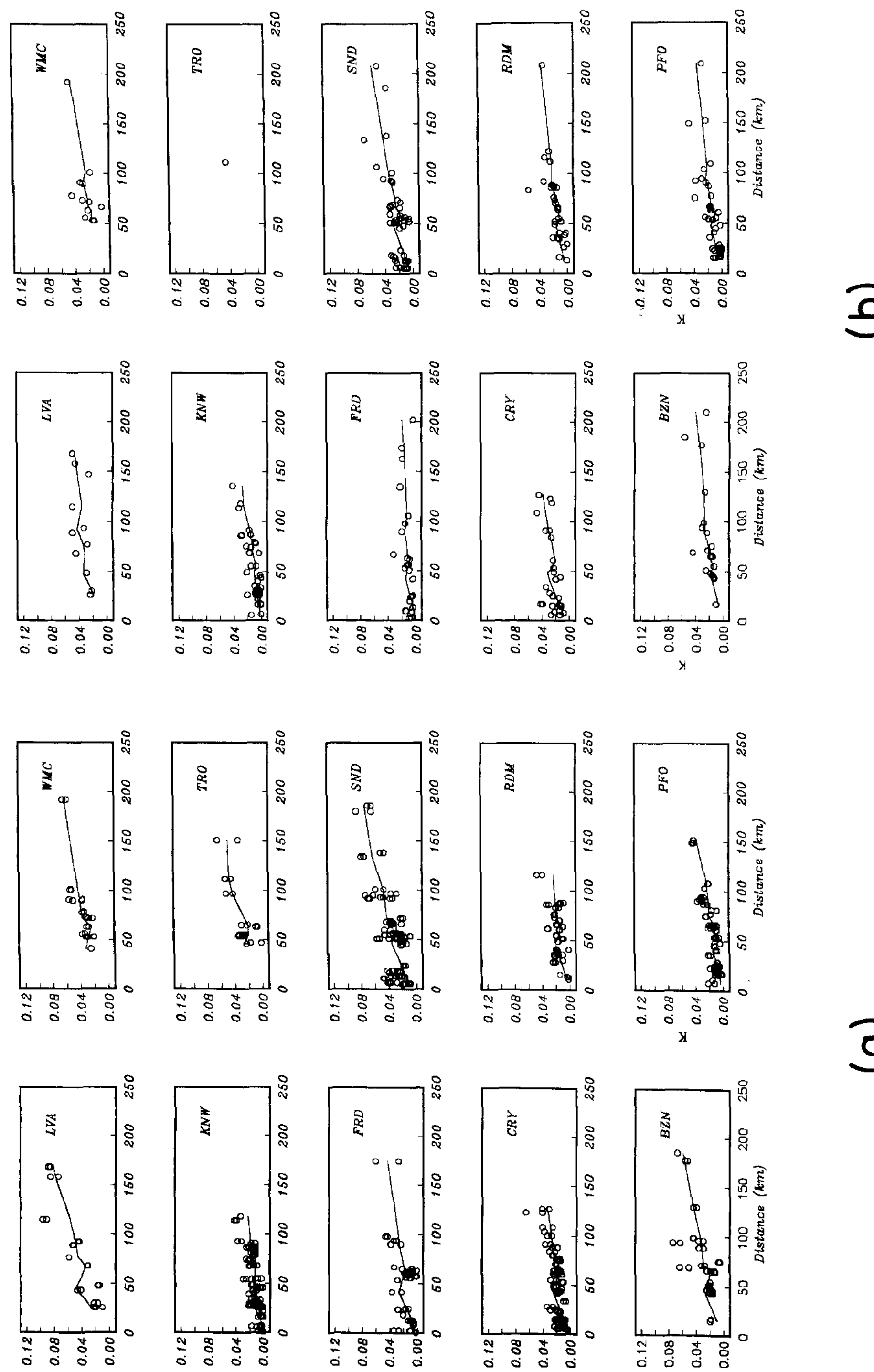

FIG. 5. Observed data at each station with predicted κ from Q_i models shown in Figure 6 (a and b).

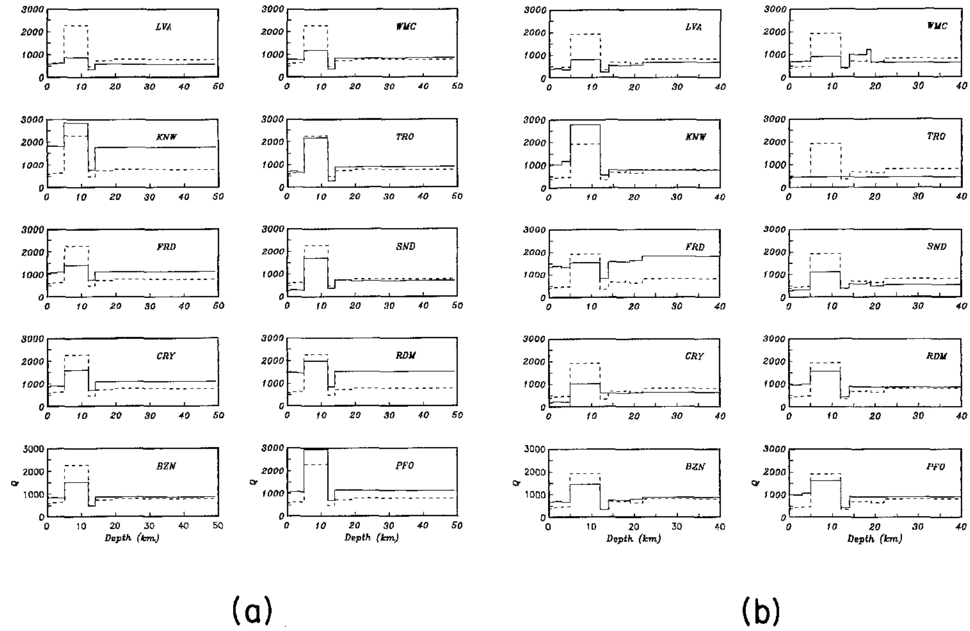

FIG. 6. Q_i models from each Anza station for shear waves and P waves [(a) and (b) respectively].

50 to 60 km. The combined, smoothed S-wave data is an excellent example, as are the P-wave data sets at KNW, FRD, and PFO. To fit this feature and a nonzero intercept more closely, one could allow a jump from a low Q_i surface layer to a layer in which Q_i is infinite. At least some of the data sets are therefore not inconsistent with a model which has an infinite Q_i layer between, say, 5 and 12 km. The models shown in Figures 3, 4, and 6 are the models which come as close as possible to being constant with depth while still giving an acceptable level of misfit from the observations. In order to achieve these models, we are forced to accept slightly higher misfit between the data and the predicted κ from the models, but Figure 2 illustrates that a large reduction in model size can be obtained with very small increases in misfit.

Since the data are large distances is sampling regional structure, we do not expect significant differences in the Q_i models derived at each station for depths greater than 10 to 12 km. The models in Figure 6 (a and b) are fairly consistent at these depths. In three cases, the inversion yielded a higher Q_i than average below 12 km (KNW S waves, RDM S waves, and FRD P waves). For the S-wave cases, there is very little distant data controlling the models at depth (Figure 5), and so the inversion procedure is giving a high Q_i in order to achieve smoother models.

COMPARISON WITH HOUGH *ET AL.* (1988)

In Hough *et al.* (1988), we demonstrated that values of Q obtained from the spectral parameterization [equation (1)] are consistent with total Q obtained from the spectral amplitude technique. To accomplish this, we merely associated $d\kappa/dr$ with $\frac{1}{Q_i}$ at the depths of lateral propagation, i.e., greater than approximately 5 km. We did not anticipate the results, obtained here, that a three-layer model would be called for by the data.

It turns out that the average value of $d\kappa/dr$, as obtained from the linear regressions through the estimated κ values in Hough *et al.* (1988), implies a value of Q_i which

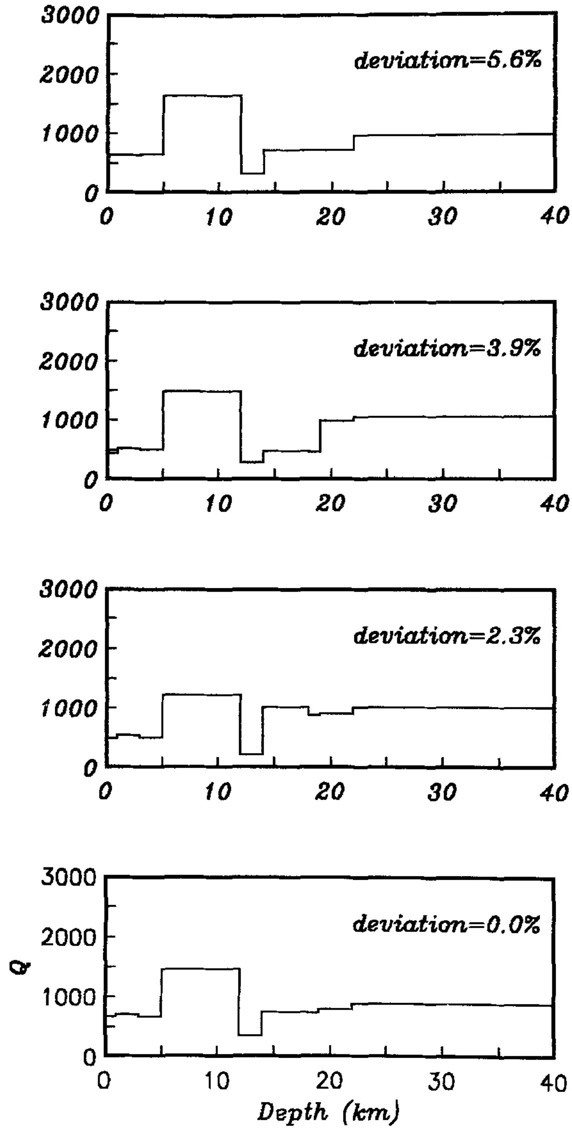

FIG. 7. *P*-wave Q_i models for station BZN derived using the initial velocity model (*bottom*) and velocity models which are perturbed by 2 to 6 per cent.

lies in between the values of Q_i for the 5 to 12 km depths and the values for greater than 12 km depths obtained in the present inversion. This is true for the average models and for most of the inversions from individual stations as well. The result makes sense, as $d\kappa/dr$ would tend to average the slopes in the near-flat segment of κ versus r (zero to approximately 60 km) and the faster increase at greater distances. Although we would like to obtain Q_d as a function of depth, to do so will require either more data from similar-sized earthquakes at a large range of distances or the introduction of a model for scaling of earthquakes. While we hope to do this in the future, it was not attempted in this study. Thus, although the new results are consistent with our conclusions about the comparison of Q_t using the two techniques in Hough *et al.* (1988), we do not have sufficient information to extend that comparison to individual layers in our inversion results.

Uncertainties and Limitations of the Q Inversion

We will note some of the limitations of our inversion procedure in this section. Overly simple assumptions will lead to errors which are difficult to quantify. In our inversion, they are leading to both Q_i models and predicted $\kappa(r)$ curves which have a more detailed structure than the data support. We do not believe that the Earth produces $\kappa(r)$ curves with sharp dips and jumps, or that there is a resolvable 1- to 2-km-thick low Q_i zone at 12 to 14 km depth. However, the formal inversion allows us to maximize the smoothness of our Q_i models in a way which depends not on vague personal judgment but instead on quantifiable criteria. Despite the limitations, our final results combining Q_i and Q_d agree well with our independent estimate of total Q. It thus appears that we have been successful in determining the gross properties of Q_i and Q_d.

The predicted $\kappa(r)$ curves in Figure 5 are not particularly smooth. While a smooth Q_i model generally implies a smooth $\kappa(r)$ profile along one branch of a travel-time curve, this is not the case when there is a transition to rays which turn at a different layer. The peculiar structure in the predicted curves at distance near 50 km is due to a transition from direct waves to rays which leave the source going downward. This illustrates a limitation of our inversion procedure; by distances of 170 km, the S wavetrain becomes dominated by Lg phases (Bouchon, 1982). The inversion assumes that the fastest ray path is representative of the actual path, but as noted, the time windows are long enough to include a greater range of group velocities.

Thus, in our inversion, there is a transition from direct waves to waves which have turned at depth which is artificially abrupt. The consequence of these will be evaluated by the use of synthetic seismograms in research now in progress.

Our inversion procedure is also sensitive to the velocity model. The ray paths depend on the velocity structure in a very nonlinear way, so it is difficult to determine what effect a perturbation of $v(z)$ will have on $Q_i(z)$. Neither do we know how big a perturbation in $v(z)$ should be considered because rigorous error bounds for the velocity model are not known. Velocity bounds can be computed from $\tau - p$

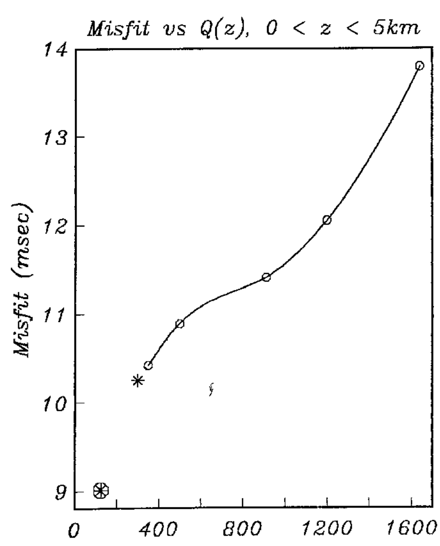

FIG. 8. Misfit in milliseconds at station SND versus the size of Q_i (P wave) in the top 5 km of the Earth. Asterisk shows misfit from Q_i model shown in Figure 6b. Circled asterisk shows misfit from three-layer model with infinite Q_i layer between 5 and 12 km.

data (e.g., Bessoneva *et al.*, 1974, 1976; Johnson and Lee, 1985; Stark *et al.*, 1986), but for the Anza region, it is difficult to estimate even two or three $\tau(p)$ values because the travel-time curve is nearly linear.

Given the lack of rigorous error bounds on the velocity models, we show that the Q_i models are not critically sensitive to uncertainties in $\nu(z)$ that are on the order that one might expect, say 2 to 5 per cent. One does not want to consider models that are everywhere 5 per cent higher or lower than the original model because these models will not fit the travel-time data. To be more realistic, three velocity models were randomly generated such that

$$\frac{1}{d_t}\sum_{i=1}^{i=N}\frac{(|\nu_{new}-\nu_{init}|)}{\nu_{init}}\,\delta d_i = 2\text{–}6 \text{ per cent} \tag{7}$$

where δd is the layer thickness, ν_{new} and ν_{init} are the new and modified velocities in each layer, and d_t is the total depth of the model. The resulting Q_i models for these three velocity models are shown in Figure 7. The data shown are S-wave data from station BZN. We conclude that the two-layer structure in the top 10 to 12 km of our models is insensitive to small changes in $\nu(z)$, although we have not proven that this must always be the case. The low Q_i layer at depth is apparently more sensitive to the velocity model, although the feature persists in 3 of the 4 Q_i models shown in Figure 7.

We applied another test to evaluate whether an increase of Q_i with depth in the upper 10 km is necessary. Specifically, we examine how well can the data be fit if one forces Q_i to be higher in the top few kilometers. This is not rigorous for a number of reasons, most fundamentally that this penalty contradicts the requirement that $1/Q_i$ be smooth. This procedure shows that a low Q_i layer of 800 over a bottom layer with $Q_i = 1200$ is not very well resolved; the top 5 km can have the same Q_i as the layers below with very little increase is misfit. This is not surprising given the very small difference in amplitudes that results from a range of Q_i between 800 and 1200 over 5 km. The low Q_i layer at SND, however, is $\approx$300 and misfit increases substantially as this value is forced to increase. Figure 8 shows the level of misfit plotted against size of Q_i in the top 5 km at SND, and Figure 8 shows the predicted values of κ from a Q_i model at SND which has no low Q_i layer near the surface. The data at SND show a nonzero $\kappa(0)$ and a slow increase of $\kappa(r)$ over the first 50 km, features which demand a two-layer interpretation with a large jump in Q_i. Suppressing this jump leads to a model with lower Q_i over 0 to 12 km than the original model has from 5 to 12 km, yielding a steeply rising predicted $\kappa(r)$ curve. Thus, the observations are poorly fit for $d \leqq 50$ km, and we conclude that the low Q_i layer is convincingly resolved at SND. This definitive result is not due to higher data quality at SND than at other Anza stations, but rather to the fact that there is simply more variation of $Q_i(z)$ at SND than at most of the stations.

A similar procedure can be used to determine the significance of the low Q_i values at depths greater than 12 to 14 km. Figure 9 shows the predicted κ values for P waves at PFO when Q_i at depth is forced to be $\approx$1900 instead of 1100, as predicted by the inversions. Again, we note that the data are not well fit by the higher Q_i model.

Included in Figures 8 and 10 are results from a three-layer model for S waves in which Q_i is set to 125 from 0 to 5 km, to infinity from 5 to 12 km, and to 850 from 12 to 40 km. In Figure 8, we see that allowing an infinite Q_i layer has a smaller misfit than the most nearly constant model. The improvement in fit is relatively

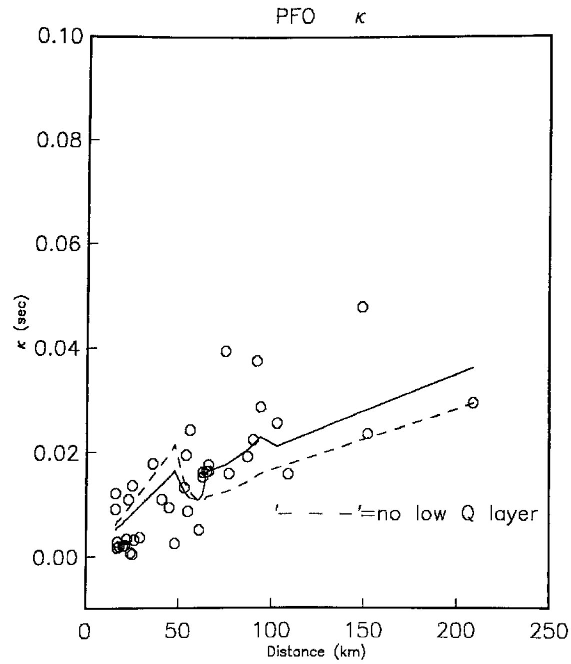

FIG. 9. Solid line shows predicted κ at PFO from Q_i model shown in Figure 6a. Dashed line shows predicted κ from model with no low Q layer at depths greater than 15 km.

small, although the fit might be improved by further adjusting the Q_i model. Figure 10 shows that the $\kappa(r)$ curve predicted from this three-layer model is smoother than the other two curves shown. This illustrates our earlier point that the data are not inconsistent with an infinite Q_i layer between 5 and 12 km; they also do not require it. We note, however, that the overall differences between the three-layer model and the most nearly constant model for SND are small. Our most nearly constant model may be approximated by another three-layer model with a Q_i of 300 between 0 and 5 km, 1500 between 5 and 12 km, and 600 between 12 and 40 km. The true values of Q_i are likely to lie somewhere in between these two models; the Earth is not likely to have a layer in which Q_i is infinite, but our most nearly constant model yields an implausible predicted $\kappa(r)$ curve. Given the small contribution to attenuation caused by a 7-km-thick layer with Q_i of 1500, $\kappa = 0.0016$, compared to a κ of zero caused by an infinite Q_i layer, this range is not unreasonably large; Q_i^{-1} is bracketed between 0.0008 and 0. The difference between a surface layer Q_i of 125 or 300 is more significant, but this level of uncertainty is not surprising given the high level of scatter at SND.

Mechanism of Attenuation

The physical mechanism for Q is not completely understood. It is not known, for instance, whether observed attenuation is mainly due to scattering or to intrinsic attenuation. This paper has obtained two classes of results that are important for the identification of the mechanism of Q. The first is the depth dependence of Q. The second is the frequency dependence and ratio of Q_P to Q_S.

The depth dependence of Q_i gives the strongest clue. Specifically, Q_i is apparently correlated with the resistance of the crustal rocks to shear faulting (Figure 11). Sibson (1983) has previously demonstrated the relationship between theoretical shear resistance and earthquake depths which is illustrated in Figure 11. The

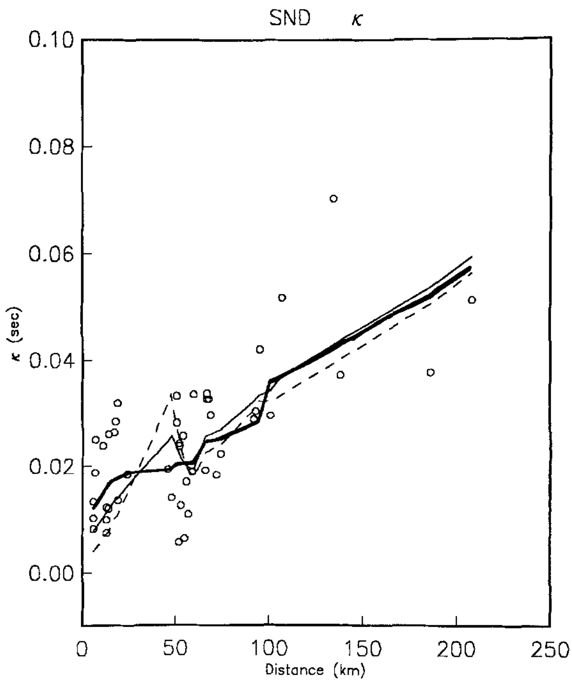

FIG. 10. Light solid line shows predicted κ of SND from Q_i model in Figure 6b. Dashed line is from model with no Q layer for $0 \leqq z \leqq 5$ km. The observed values of κ at distances less than 50 km are poorly fit when there is no low Q layer. The heavy solid line shows predicted κ from three-layer model with infinite Q_i layer.

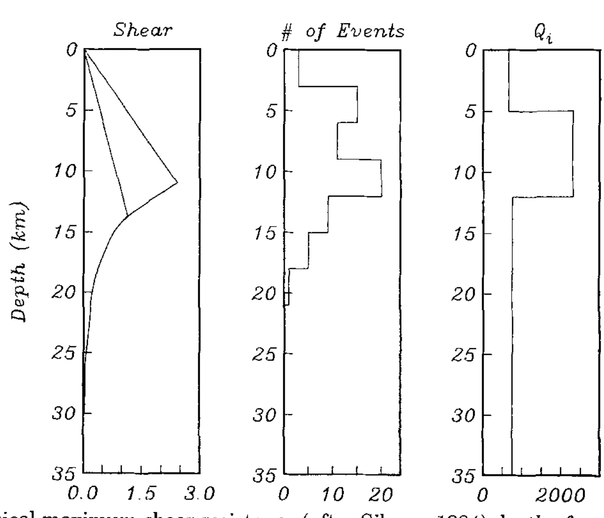

FIG. 11. Theoretical maximum shear resistance (after Sibson, 1984) depth of earthquakes near Anza (after Doser and Kanamori, 1986), and Q_i as a function of depth. Shear resistance is in kilobars. The Q_i model is an idealized three-layer model for S waves, with values taken from Figure 4a.

correlation between our estimate for Q_i and the depths of earthquakes is particularly striking. Our results indicate that the seismogenic zone is less attenuating than the material at greater depth and thus suggest a relationship between Q_i and shear resistance.

Thus, Q_i might be due to an intrinsic loss mechanism which depends on temperature and pressure. Given that there are not likely to be major changes in rock type within the southern California batholith between 0 and 10 km depth, we consider it likely that our observed increase of Q_i in the shallow layer is due to increasing pressure. The hydrostatic pressure at 5 km is 1000 to 1500 bars, and laboratory studies generally show an increase of intrinsic Q for pressures between 0 and 1000 bars (e.g., Johnston, 1981). As noted, the decrease of Q_i at the base of the seismogenic zone corresponds to the depth at which shear resistance decreases due to increasing temperature. However, attributing this decrease of Q_i solely to temperature is more speculative because there are potentially other changes, such as a change of rock type, occurring at this depth.

The result that Q_i is higher for S waves than for P waves is also potentially useful in distinguishing between different attenuation mechanisms. The ratio of Q_S/Q_P includes both depth and frequency dependence and varies with frequency because of the frequency-dependent component of Q. For depths typical of lateral propagation, 12 to 40 km, Hough *et al.* (1988) report that Q_S/Q_P has a representative value of ≈ 1.2, with a similar value obtained for Q_d independently. In our new results for $Q_i(z)$, the ratio depends on depth and is somewhat difficult to assess, although Figure 6 shows that Q_{iS} is generally slightly higher than Q_{iP}. The results from the combined, smoothed data sets are that Q_{iS} is higher than Q_{iP} from 0 to 12 km by a factor of 1.2 to 1.5. Q_{iS} is comparable to Q_{ip} at greater depths. Q_S/Q_P ratios of 1.0 to 1.5 are in rough agreement with the ratios obtained from high-frequency studies in other locations (Table 1). Knopoff (1964) also presents a summary of numerous attenuation studies, several of which also report $Q_S \geqq Q_P$.

In theoretical studies, the value of Q_S/Q_P depends on the attenuation mechanism. As examples, Sato (1984) predicts $Q_S/Q_P = 2.4$ for Rayleigh scattering at high frequencies, and Richards and Menke (1983) give $Q_S/Q_P \approx 1$ for plane-layer scattering. Anderson *et al.* (1965) show that, for intrinsic shear losses, Q_S/Q_P is $\frac{4}{3}(v_S/v_P)^2$ or $\approx \frac{4}{9}$. Laboratory measurements typically show $Q_S/Q_P < 1$ for intrinsic attenuation in water-saturated rock, and $Q_S/Q_P > 1$ in dry rock (e.g., Toksöz *et al.*, 1978; Johnston, 1981). It thus may be that $Q_S/Q_P \geqq 1$ is to be expected for most kinds of scattering but that the theoretical ratio for intrinsic absorption is somewhat uncertain. This uncertainty limits the usefulness of a Q_S/Q_P ratio in discriminating between attenuation mechanisms.

The appearance of the seismograms at Anza demonstrates that scattering is occurring and is qualitatively stronger at some stations than others as a physical mechanism for Q. Figure 12 shows one channel of a magnitude 4 event which was recorded at nine Anza stations. The simple waveforms observed at the least-attenuating stations, particularly KNW, are qualitatively different than the more complex, generally longer-lasting arrivals observed at stations like SND and WMC. Intrinsic attenuation would lower the amplitude of the first arrival and broaden the width of an input pulse, but it would not cause the observed complexity of arrivals.

TABLE 1

Q_S/Q_P REPORTED BY PREVIOUS STUDIES FOR DIFFERENT LOCATIONS

Q_S/Q_P	Frequency (Hz)	Area	Reference
0.6	10–35	San Andreas	Bakun *et al.*, 1976
1.73	1–20	Central Asia	Rautian *et al.*, 1978
1.0	5–20	Caribbean	Frankel, 1982
1.6	20–50	Pyrenees	Modiano and Hatzfeld, 1982
0.8–1.85	20–40	West Germany	Hoang-Trong, 1983
0.9–1.5	3–25	Baja California	Rebollar *et al.*, 1985

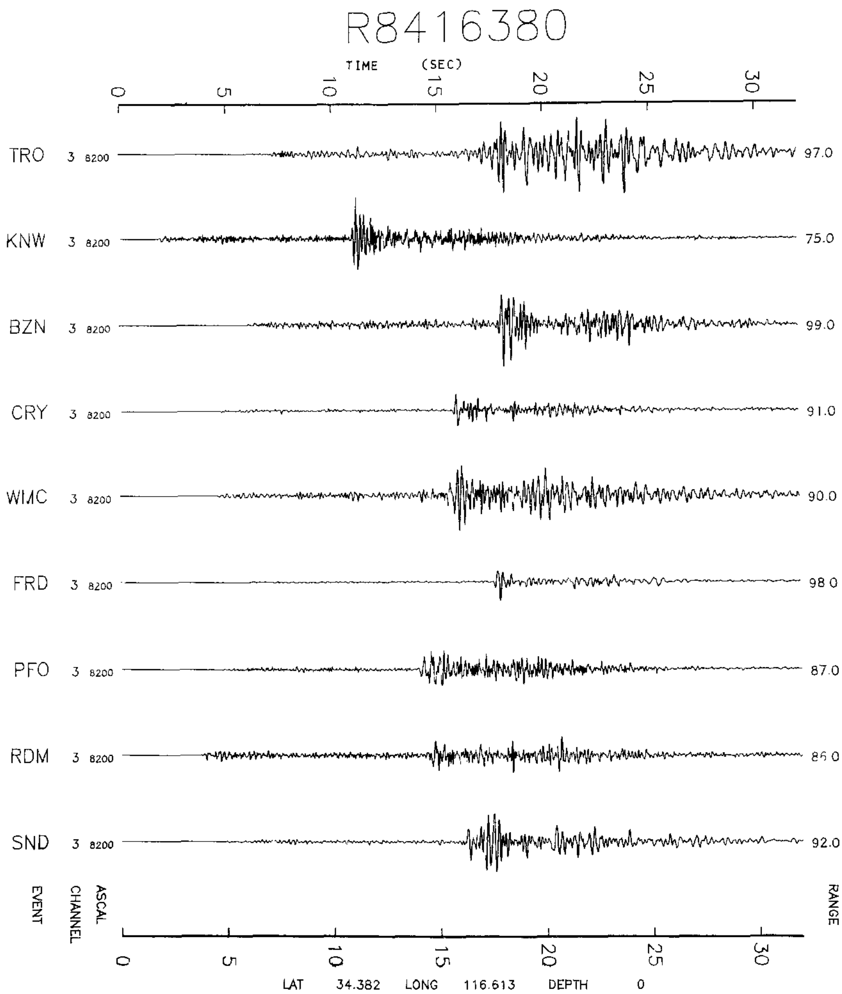

FIG. 12. Seismograms from a magnitude 4.0 event which occurred roughly 90 km north of the Anza array. All traces are plotted at the same vertical scale and are horizontal components. The station codes are to the *left* of each trace (see Hough *et al.*, 1988).

We have not shown that the two components of Q, Q_i and Q_d, are caused by different mechanisms. Given the above considerations, however, we conclude that it is likely that the observed attenuation at Anza is due to two or more different mechanisms. The depth dependence of Q_i suggests an intrinsic loss mechanism controlled by heat and pressure, while qualitative observations of seismograms suggest that a scattering mechanism also removes energy from the initial wave arrivals. Although some studies of scattering mechanisms find that scattering yields Q independent of frequency (e.g., Richards and Menke, 1983; Frankel and Clayton, 1986), we tentatively identify Q_d as the component of Q which is due to scattering. For frequencies less than 20 to 25 Hz, the bigger contribution to total Q comes from this frequency-dependent component.

Discussion

Observations of the spectral decay parameter as a function of distance have been inverted to find Q_i models which are both smooth and consistent with the data. The solutions have an increase of Q_i at $\approx$5 km depth. Given the high values of Q_i near the surface at most Anza stations, the resolution of a lower Q_i layer at any one station is difficult to prove. However, the persistence of this type of solution is an argument for its validity, as is the fact that the values of Q_i in the surface layers at the 10 Anza stations correlate with the geological conditions at each station. The low Q_i layer is convincingly resolved at station SND, a station which one expects to have higher than average attenuation because it is located on sheared material in the San Jacinto fault zone.

The high Q_i region at intermediate depths is required by the very slow increase of κ over distances from 0 to 50 km (see Figure 4) and is perhaps the best-resolved feature of the models. We note, however, that the numerical value of Q_i in this layer is not necessarily well resolved because the total contribution to κ from that depth range is very small. Even though the Anza region is in the midst of a batholith and there is no reason to expect any change in rock composition in the upper 10 to 20 km, the data are not explained by a model in which Q_i is constant with depth.

Perhaps our most important conclusion is the recognition that Q_i has a peak at seismogenic depths, and the suggestion that it may be correlated therefore with the shear resistance. It would be interesting to see if this correlation holds in the Eastern United States as well, where heat flow is lower and earthquakes are observed at greater depths than in the Western United States.

Acknowledgments

We are grateful to Jim Brune for many helpful discussions and suggestions, to Frank Vernon for assistance with the data, and to Bob Parker for advice pertaining to the inversion procedure. We also acknowledge the helpful comments by Jerry King, J. E. Luco, and W. Menke. Work was supported by the Electric Power Research Institute Project RP2556-2 and National Science Foundation Grants EAR84-08429 and CEE83-19620.

References

Anderson, D. L., A. Ben-Menahem, and C. B. Archambeau (1965). Attenuation of seismic energy in the upper mantle, *J. Geophys. Res.* **70,** 1441–1445.

Backus, G. and F. Gilbert (1968). The resolving power of gross Earth data, *Geophys. J. R. Astr. Soc.* **16,** 169–205.

Backus, G. and F. Gilbert (1970). Uniqueness in the inversion of inaccurate gross Earth data, *Phil. Trans. R. Soc. Lond.* **266A,** 123–192.

Bakun, W. H., D. G. Bufe, and R. M. Stewart (1976). Body-waves spectra of central California earthquakes, *Bull. Seism. Soc. Am.* **66,** 363–384.

Bessoneva, E. N., V. N. Fishman, V. Z. Ryaboyi, and G. A. Sitnikova (1974). The tau method for inversion of travel times. I. Deep seismic sounding data, *Geophys. J. R. Astr. Soc.* **36,** 377–398.

Bessoneva, E. N., V. N. Fishman, M. G. Shnirman, G. A. Sitnikova, and L. R. Johnson (1976). The tau method for inversion of travel times. II. Earthquake data, *Geophys. J. R. Astr. Soc.* **46,** 87–108.

Bouchon, M. (1982). The complete synthesis of seismic crustal phases at regional distances, *J. Geophys. Res.* **87,** 1735–1742.

Doser, D. and H. Kanamori (1986). Depth of seismicity in the Imperial Valley Region (1977–1983) and its relationship to heat flow, crustal structure, and the October 15, 1979 earthquake, *J. Geophys. Res.* **91,** 675–688.

Frankel, A. (1982). The effects of attenuation and site response of the spectra of microearthquakes in the northeast Caribbean, *Bull. Seism. Soc. Am.* **72,** 1379–1402.

Frankel, A. and R. W. Clayton (1986). Finite difference simulations of seismic scattering: implications for the propagation of short-period seismic waves in the crust and models of crustal heterogeneity, *J. Geophys. Res.* **91,** 6465–6489.

Hoang-Trong, P. (1983). Some medium properties of the Hohenzollergraben (Swabian, Jura, W. Germany) inferred from Q_P/Q_S ratio analysis, *Physics Earth Planet. Interiors* **31,** 119–131.

Hough, S. E., J. G. Anderson, J. Brune, F. Vernon, III, J. Berger, J. Fletcher, L. Haar, T. Hanks, and L. Baker (1988). Attenuation near Anza, California, *Bull. Seism. Soc. Am.* **78,** 672–691.

Johnson, L. R. and R. C. Lee (1985). External bounds on the *P* velocity in the Earth's core, *Bull. Seism. Soc. Am.* **75,** 115–130.

Johnston, D. H. (1981). Attenuation: a state-of-the-art summary, seismic wave attenuation, SEG publication.

Knopoff, L. (1964). *Q*, *Rev. Geophys.* **2,** 625–660.

Modiano, T. and D. Hatzfeld (1982). Experimental study of the spectral content for shallow earthquakes, *Bull. Seism. Soc. Am.* **72,** 1739–1758.

Rautian, T. G., V. I. Khalturin, V. G. Martinov, and P. Molnar (1978). The use of coda for determination of the earthquake source spectrum, *Bull. Seism. Soc. Am.* **68,** 949–972.

Rebollar, C. J., C. Traslosheros, and R. Alvarez (1985). Estimates of seismic wave attenuation in Northern Baja California, *Bull. Seism. Soc. Am.* **75,** 1371–1382.

Richards, P. G. and W. Menke (1983). The apparent attenuation of a scattering medium, *Bull. Seism. Soc. Am.* **73,** 1005–1021.

Sato, H. (1984). Attenuation and envelope formation of three-component seismograms of small local earthquakes in randomly inhomogeneous lithosphere, *J. Geophys. Res.* **89,** 1221–1241.

Sibson, R. H. (1983). Continental fault structure and the shallow earthquake source, *J. Geol. Soc. Lond.* **140,** 741–767.

Sibson, R. H. (1984). Roughness at the base of the seismogenic zone: contributing factors, *J. Geophys. Res.* **89,** 5791–5799.

Stark, P. B., R. L. Parker, G. Masters, and J. A. Orcutt (1986). Strict bounds on seismic velocity in the spherical Earth, *J. Geophys. Res.* **91,** 13892–13902 .

Toksöz, M. N., A. H. Johnston, and A. Timur (1978). Attenuation of seismic waves in dry and saturated rocks. I. Laboratory measurements, *Geophysics* **44,** 681–690.

INSTITUTE OF GEOPHYSICS AND PLANETARY PHYSICS (A-025)
SCRIPPS INSTITUTE OF OCEANOGRAPHY
UNIVERSITY OF CALIFORNIA, SAN DIEGO
LA JOLLA, CALIFORNIA 92093 (S.E.H., J.G.A.)

Manuscript received 15 May 1987